

Geophysical Research Letters

RESEARCH LETTER

10.1029/2020GL091624

Key Points:

- Surface wave phase delays were inverted to create a 3D shear-wave velocity model of the upper mantle beneath southern Africa
- Kalahari Craton lithosphere is defined by high velocities (~4.7–4.8 km/s) beneath the Archean cratons and surrounding Proterozoic terranes
- Upper mantle velocity structure shows little evidence for present-day thermal anomalies supporting the Southern African Plateau

Supporting Information:

Supporting Information may be found in the online version of this article.

Correspondence to:

A. L. White-Gaynor,
alw361@psu.edu

Citation:

White-Gaynor, A. L., Nyblade, A. A., Durrheim, R. J., Raveloson, R., van der Meijde, M., Fadel, I., et al. (2021). Shear-wave velocity structure of the Southern African upper mantle: Implications for craton structure and plateau uplift. *Geophysical Research Letters*, 48, e2020GL091624. <https://doi.org/10.1029/2020GL091624>

Accepted 8 FEB 2021

Shear-Wave Velocity Structure of the Southern African Upper Mantle: Implications for Craton Structure and Plateau Uplift

A. L. White-Gaynor¹ , A. A. Nyblade¹ , R. J. Durrheim² , R. Raveloson², M. van der Meijde³ , I. Fadel³ , H. Paulssen⁴ , M. Kwadiba⁵, O. Ntibinyane⁵, N. Titus⁶, and M. Sitali⁶

¹Department of Geosciences, The Pennsylvania State University, University Park, PA, USA, ²School of Geosciences, The University of Witwatersrand, Johannesburg, South Africa, ³University of Twente, Enschede, Netherlands, ⁴Utrecht University, Utrecht, Netherlands, ⁵Botswana Geosciences Institute, Lobatse, Botswana, ⁶Geological Survey of Namibia, Windhoek, Namibia

Abstract We present a 3D shear-wave velocity model of the southern African upper mantle developed using 30–200 s period Rayleigh waves recorded on regional seismic networks spanning the subcontinent. The model shows high velocities (~4.7–4.8 km/s) at depths of 50–250 km beneath the Archean nucleus and several surrounding Paleoproterozoic and Mesoproterozoic terranes, placing the margin of the greater Kalahari Craton along the southern boundary of the Damara Belt and the eastern boundaries of the Gariep and Namaqua-Natal belts. At depths ≥ 250 km, there is little difference in velocities beneath the craton and off-craton regions, suggesting that the cratonic lithosphere extends to depths of about 200–250 km. Upper mantle velocities beneath uplifted areas of southern Africa are higher than the global average and significantly higher than beneath eastern Africa, indicating there that is little thermal modification of the upper mantle present today beneath the Southern African Plateau.

Plain Language Summary We present a 3D shear-wave velocity model of the southern African upper mantle developed by modeling phase velocities of surface waves recorded on regional seismic networks spanning the African subcontinent. The model shows high velocities to depths of 250 km beneath the core of the Southern African Shield. At depths ≥ 250 km, the model shows little difference in velocities under most of southern Africa suggesting that the thickest lithosphere does not extend deeper than that. The model also shows that upper mantle velocities beneath the uplifted areas are not anomalous, indicating that there is little thermal alteration of the upper mantle present today beneath the Southern African Plateau.

1. Introduction

The Precambrian shield of southern Africa, much of which has been uplifted to form the ~1 km high Southern Africa Plateau (Nyblade & Robinson, 1994), has been the focus of many seismological studies over several decades addressing fundamental questions about continental structure and evolution, including craton formation, mantle plumes, flood basalts, rifting, and epeirogenic plateau uplift. Much of the plateau uplift may have occurred in the late Cretaceous (Baby et al., 2020; Braun et al., 2014; Stanley et al., 2013, 2015), with east to west variations in the amount and timing of uplift across the plateau (Braun et al., 2014; Stanley et al., 2020), and an additional phase of uplift may have occurred in the mid-Cenozoic (Baby et al., 2020; Braun et al., 2014). The two main sources of uplift debated are upper mantle plume heads and anomalous structure in the midmantle and lower mantle associated with the African Superplume (e.g., Baby et al., 2020; Braun et al., 2014; Gurnis et al., 2000; Nyblade & Sleep, 2003).

Most seismological studies of southern Africa (e.g., Adams & Nyblade, 2011; Chevrot & Zhao, 2007; Fouch et al., 2004; James et al., 2001; Kachingwe et al., 2015; Li, 2011; Li & Burke, 2006; Youssof et al., 2015) have focused on crustal and upper mantle structure beneath the region's Archean nucleus, largely because much of the broadband seismic data collected over the past few decades have come from networks located within the Kaapvaal and Zimbabwe cratons. Expanding on these earlier studies, in this paper, we use a large data

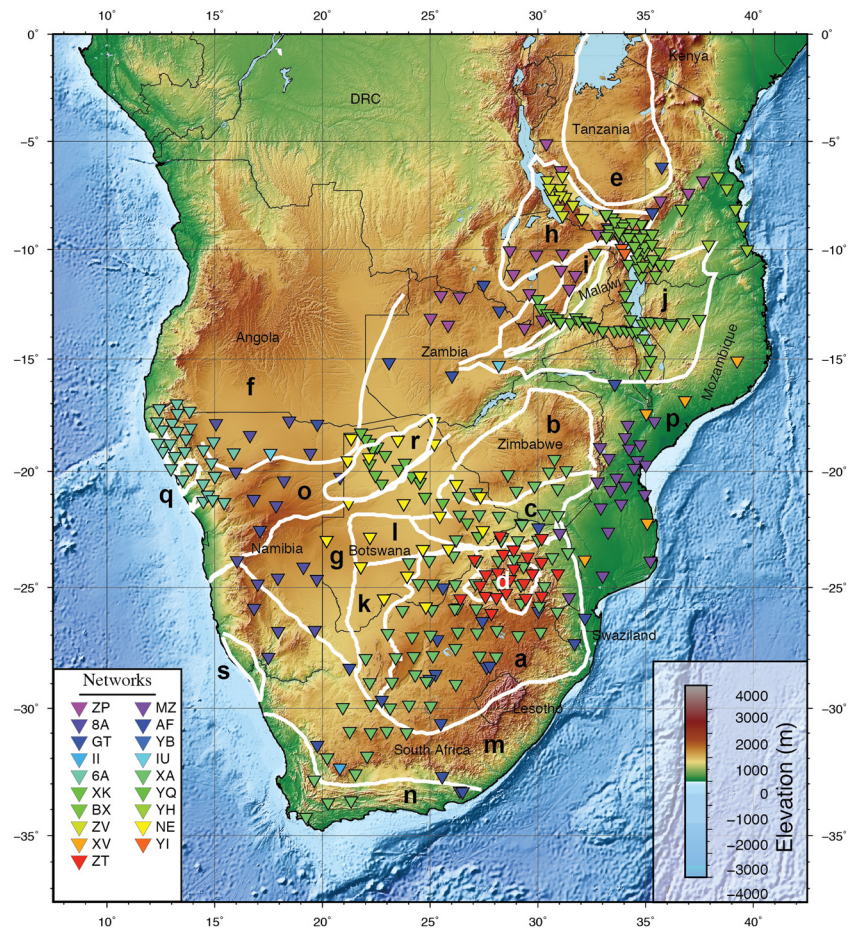


Figure 1. Topographic map showing tectonic boundaries (bold white lines) in southern and eastern Africa and locations of seismic stations used in this study. Tectonic terranes are labeled as (a) Kaapvaal Craton; (b) Zimbabwe Craton; (c) Limpopo Belt; (d) Bushveld Igneous Province; (e) Tanzania Craton; (f) Congo Craton/Angolan Shield; (g) Rehoboth Province; (h) Bangweulu Block; (i) Irumide Belt; (j) Southern Irumide Belt; (k) Kheis Belt; (l) Okwa Terrane; (m) Namaqua-Natal Belt; (n) Cape Fold Belt; (o) Damara Belt; (p) Mozambique Belt; (q) Etendeka Flood Basalt Province; (r) Okavango Rift; (s) Gariep Belt (Begg et al., 2009; Frimmel & Frank, 1998). Elevations from GEBCO (Weatherall et al., 2015).

set assembled from networks that span the southern African subcontinent from east to west to model the shear-wave velocity structure of the upper mantle beneath the entire Precambrian shield of southern Africa.

To create our shear-wave velocity model, we produced phase velocity maps by inverting Rayleigh wave phase delays from 499 $M \geq 6$ earthquakes. Dispersion curves, extracted from the maps, were modeled using a combined Monte Carlo and iterative linearized inversion approach to obtain 1D velocity models at every half degree across the study area, and then the 1D models were assembled into a 3D model. Variations in upper mantle velocities revealed in the 3D model are used to address several first-order questions about the nature of the African upper mantle, including the location of lithospheric boundaries, the thickness of cratonic lithosphere, and whether or not the sublithospheric mantle is thermally modified, thus advancing our understanding of earth structure and processes in this tectonically unique part of the world.

2. Background

The Precambrian shield of southern Africa consists of an amalgamation of cratons and mobile belts (Begg et al., 2009; de Wit et al., 1992; Hanson, 2003; Jelsma & Dirks, 2002) (Figure 1). The core of the shield consists of the Archean Kaapvaal and Zimbabwe cratons sutured together by the Limpopo Belt, a region commonly referred to as the Kalahari Craton. Around the periphery of this core are Paleoproterozoic (Kheis,

Rehoboth), Mesoproterozoic (Magondi, Okwa, Namaqua-Natal, Irumide, Southern Irumide Belts), and Neoproterozoic (Damara-Ghanzi-Chobe, Gariep, Mozambique Belts) terranes (Figure 1). The region experienced two major Phanerozoic magmatic events (the ca. 130 Ma Etendeka Flood Basalt Province within the Damara Belt in northwestern Namibia, and the ca. 180 Ma Karoo large igneous province covering much of the southern African subcontinent), in addition to several Precambrian magmatic events, most notably the ca. 2.1 Ga Bushveld event within the Kaapvaal Craton (Figure 1). Karoo rifts and sedimentary basins developed across much of southern Africa during the breakup of Gondwana, and, today, rifting is ongoing within the East African Rift System, which extends to the southwest to the Okavango Rift Zone in northern Botswana and to the southeast into central Mozambique (Domingues et al., 2016; Fadel et al., 2020).

Global surface wave tomography studies primarily image regions of higher velocity in southern Africa, indicative of thick, Archean lithosphere, and regions of lower velocity in eastern Africa, representative of thermally modified upper mantle. Details of upper mantle shear-wave velocity structure in these regions are better resolved in continental-scale and regional-scale surface wave tomography models. The Priestley et al. (2008) and Fishwick (2010) continental-scale models, e.g., show upper mantle with 2–4% higher velocities to depths of 200–250 km beneath the Kaapvaal and Zimbabwe cratons compared to surrounding terranes. Emry et al. (2019) imaged, in addition to the higher velocities beneath those cratons, smaller regions of high velocity upper mantle possibly correlated with other cratonic fragments (i.e., the Niassa and Lurio cratons). Regional-scale studies also show high velocity lithospheric mantle beneath the Kaapvaal Craton (e.g., Adams & Nyblade, 2011; Chevrot & Zhao, 2007; Li, 2011; Li & Burke, 2006; Ravenna et al., 2018) but differences in velocities within the sublithospheric mantle. For instance, the Li and Burke (2006) model shows a 4% reduction in shear-wave velocities in the 160–260-km depth range beneath the Kaapvaal Craton, suggestive of thermally perturbed upper mantle, while the Adams and Nyblade (2011) model shows no low velocity region under the craton. Complementing the surface wave investigations are many other seismological studies of the crust and upper mantle beneath southern Africa (see Emry et al. (2019) and White-Gaynor et al. (2020) for recent reviews).

3. Rayleigh Wave Phase Velocities

Our shear-wave velocity model for southern Africa has been constructed by inverting Rayleigh wave phase velocity measurements for an area between -5°S to -40°S and 10°E to 40°E . Phase velocity measurements from periods of 30 to 200 s were made using the Automated Surface Wave Measuring System (ASWMS; Jin & Gaherty, 2015). Data were gathered from a total of 397 broadband seismic stations in 19 different networks (Figure 1; see data section). Waveforms were collected for ≤ 50 -km deep and $M \geq 6.0$ earthquakes with epicentral distances between 20° and 160° over the years of 1997–2018. In total, waveforms were collected from 1,419 earthquakes on all stations operational within the study area at the time of each event. Of these, 499 events provided waveforms with coherent signal within the frequency band of interest (30–200 s), providing good azimuthal coverage (Figure S1).

The ASWMS workflow uses a modified Generalized Seismological Data Functional (Gee & Jordan, 1992) approach to measure phase delays between two stations. After correcting waveforms for instrument response, a waveform from one station is cross-correlated with a waveform from the same event recorded on a nearby station, windowed using a group velocity arrival window of 5.0–2.0 km/s (Figure S2). Cross-correlograms are then filtered by a series of narrow-band filters centered around the periods of interest (20–300 s; Figure S2). Correlograms with coherences ≥ 0.5 were fit with a five-parameter Gaussian wavelet (Jin & Gaherty, 2015), of which one parameter corresponds with phase delay and one with amplitude, providing amplitude and phase delay estimates by period. Phase delays greater than 10 s from the predicted phase velocity were rejected to prevent measuring phase delays on skipped cycles. Interstation distances were extended to a maximum of 850 km to increase path coverage. For comparison, we also limited the maximum interstation distance to 250 km and found differences at all periods of generally < 0.1 km/s (Figure S3). To remove possible bias imposed by the windowing function, the phase delays were corrected by a time shift measured on a windowed autocorrelation.

Corrected phase delays were then inverted for spatial variations in dynamic phase velocity via the eikonal equation and by applying a smoothing of 25% of the wavelength at each period, following the approach

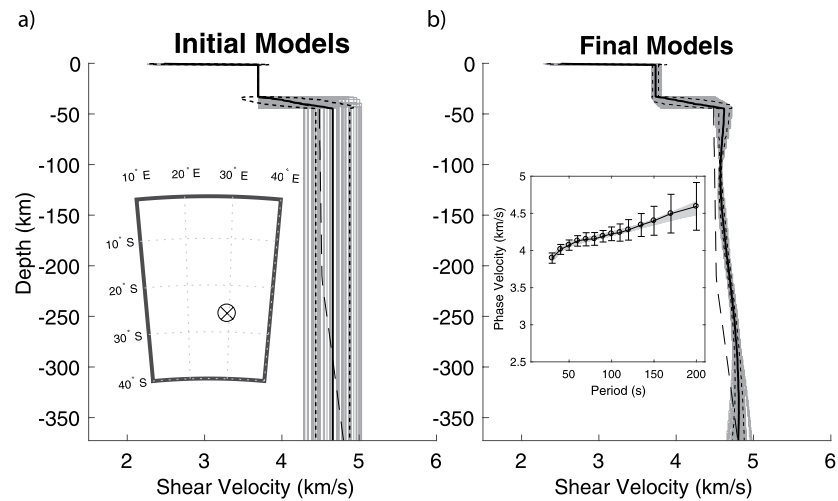


Figure 2. (a) Starting model from the grid search (black line) and 100 perturbed initial models (gray lines). One standard deviation above and below the mean is marked (dotted lines). AK135 Earth reference model shown with dashed line (Kennett et al., 1995). Cell location marked on inset map. (b) Model results from the inversion with mean (black line), one standard deviation above and below the mean (dotted lines), and individual output velocity models (gray lines). Inset: Phase velocities used to constrain the inversion along with their uncertainties from Helmholtz tomography (Figure S6). Phase velocities forward calculated for the individual velocity models are shown with gray lines.

outlined in Accardo et al. (2017). The smoothness constraint minimizes the second derivative of the slowness vector calculated from the derived maps of phase delay. A minimum of three measurements were required for the phase velocity measurements for a cell to be used in further calculations (Figure S4). The effects of focusing and defocusing were then corrected for by inverting amplitude measurements using Helmholtz tomography (Lin & Ritzwoller, 2011), yielding maps of structural phase velocity at each frequency for each event. The final event solutions were then stacked to obtain structural phase velocity estimates at all periods for every grid point (Figure S5), and the standard deviation of the resulting phase velocities (Figure S6). The standard deviations, which are generally <0.02 km/s, provide an estimate of the uncertainty. Lastly, phase velocity dispersion curves were extracted across all periods from each $0.5^\circ \times 0.5^\circ$ cell with at least three measurements.

4. Inversion for Shear-Wave Velocities

Shear-wave velocity profiles for each cell in the grid were obtained by inverting the phase velocity dispersion curves following the method of Jin et al. (2015), as implemented by Accardo et al. (2020). The inversion of dispersion curves for velocity can be sensitive to the initial velocity model, so a suite of 100 3-layer starting models for each cell was developed using a Monte Carlo approach applied to a limited parameter space (Table S1). The top layer (layer 1) was used to represent a sedimentary layer, the middle layer (layer 2) to represent the crust, and the bottom layer (layer 3) to represent the upper mantle to 400-km depth. The crustal thickness at each cell was constrained by the Tugume et al. (2013) crustal model. At the bottom of layer 3, the mantle velocity was linearly tapered to the velocity of the AK135 model (Kennett et al., 1995) at 500 km, and from 500-km to 550-km depth, velocities were fixed to the AK135 velocities. The 100 initial models for each cell were obtained by perturbing the three layers in the starting model independently. Perturbations followed a uniform distribution within 30% of the starting layer 1 velocity, 10% of the starting layer 3 velocity and 5 km of the starting crustal thickness. Average crustal velocity (layer 2) was fixed at 3.7 km/s due to the narrow distribution of crustal velocities found in southern Africa (Kachingwe et al., 2015; Tugume et al., 2013).

Each initial model (100 per cell) was then inverted using an iterative linearized inversion scheme (surf96 code; Herrmann, 2013) to obtain a 1D shear-wave velocity profile (Figure 2). Smoothing was enforced in the inversion except at the step increase in velocity at the Moho and at 500-km depth. We narrowed the

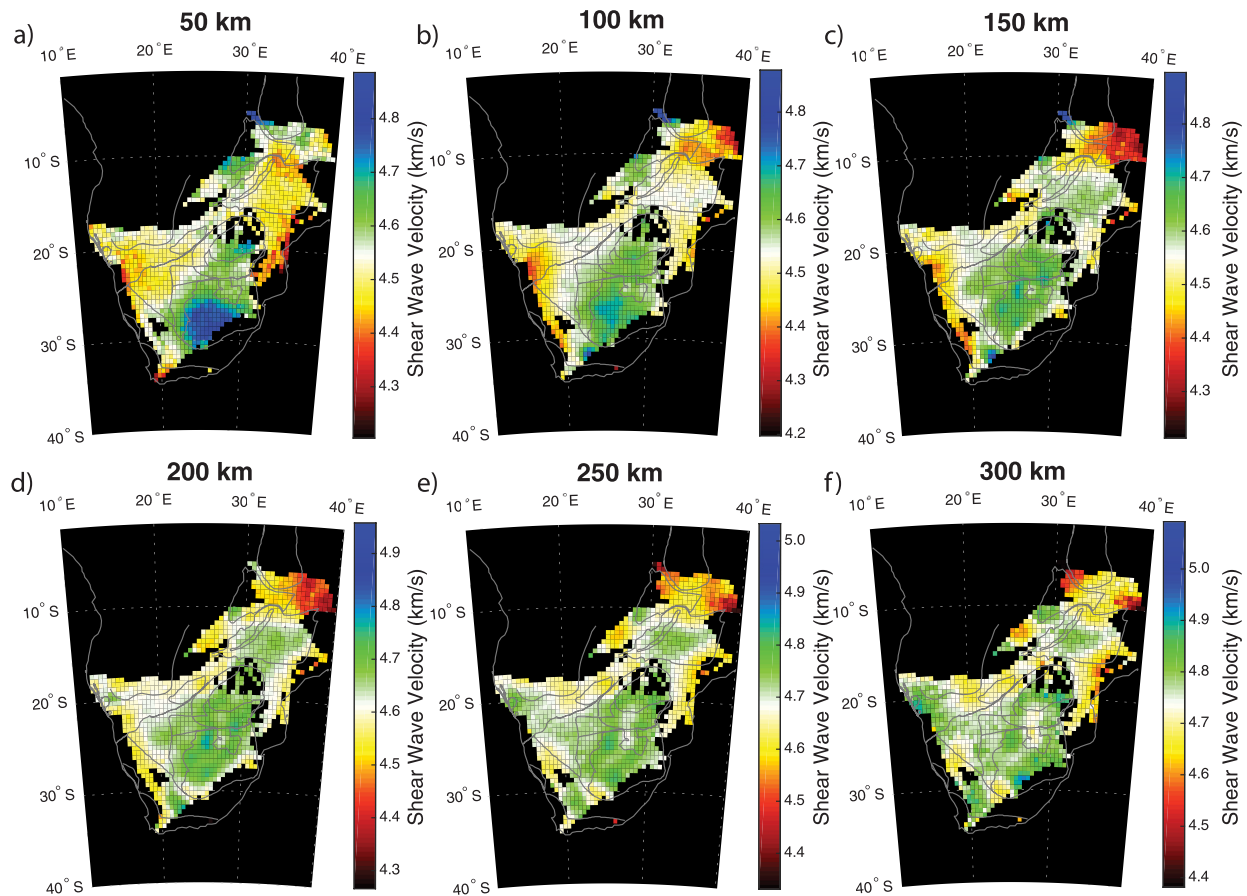


Figure 3. Horizontal cross-sections through the 3D velocity model at 50-km intervals. Terrane boundaries shown with solid gray lines are the same as in Figure 1.

distribution of resulting 1D models by excluding the 30% of models with the largest misfit, and then calculated the mean and standard deviation of the remaining models to obtain a representative 1D model for each cell. The mean velocity profiles were stable with respect to the choice of cutoff for misfit; increasing the cutoff to exclude the 50% of models with the largest misfit resulted in nearly identical velocity profiles and variance. The mean 1D velocity models were then assembled into a 3D model.

5. Results

Horizontal slices through the shear velocity model are shown in Figure 3. The Kaapvaal Craton has the highest shear-wave velocities (~ 4.8 km/s) within the uppermost mantle at 50-km depth, and at 150-km depth the maximum velocity is slightly lower (~ 4.7 km/s). Beneath the Limpopo Belt and Bushveld Complex in the northern Kaapvaal Craton, the velocities are slightly lower, ~ 4.6 km/s at depths of 50 and 150 km. Beneath the Zimbabwe Craton, velocities are slightly lower than beneath the Kaapvaal Craton, although the northern part of the Zimbabwe Craton is not well imaged because of limited data coverage. Below 200-km depth, the entire Kalahari Craton (Kaapvaal and Zimbabwe cratons and Limpopo Belt) has a shear-wave velocity between 4.7 and 4.8 km/s.

Shear-wave velocities beneath the Rehoboth Province are ~ 4.5 km/s at 50-km depth, increasing to ~ 4.6 km/s at 150-km depth and to 4.7–4.8 km/s below 200-km depth. The western portion of the province has slightly lower velocities than the eastern part of the province. To the north of the Rehoboth Province, beneath the Damara Belt in Namibia, Botswana, and Zambia shear-wave velocities are 4.4–4.5 km/s at 50-km depth. At 150-km depth, beneath the Damara Belt velocities increase to 4.5–4.6 km/s. At depths >200 km, velocities range from 4.7 to 4.8 km/s, with the highest velocities (4.8 km/s) present beneath the Etendeka Flood

Basalt Province in northwestern Namibia. Under the Okavango Rift in northern Botswana, velocities are comparable to the rest of the Damara Belt. Beneath the Mozambique Belt extending from southern Tanzania through Malawi and northern Mozambique, velocities at 50-km depth are between 4.4 and 4.5 km/s. Velocities are lower (<4.5 km/s) at all depths beneath southern Tanzania but to the south in Malawi and Mozambique, velocities increase to 4.7–4.8 km/s beneath the Southern Irumide Belt at depths of ≥ 150 km.

6. Discussion

Our shear velocity model is the first 3D model for southern Africa constructed using surface waves recorded on regional seismic networks spanning the entire subcontinent. In cratonic regions where data from regional seismic networks have been available previously, first-order features in our model are similar to other continental-scale and regional-scale shear-wave velocity models of the upper mantle (e.g., Emry et al., 2019; Fishwick, 2010; Li & Burke, 2006; Priestley et al., 2008; Ravenna et al., 2018; Sebai et al., 2006). However, because of the inclusion of new data, primarily in off-craton locations, we are able to make four important observations from our model that provide new insights into the nature of the African mantle and tectonics. To help illustrate these observations, in Figure 4, we show averages of the shear-wave velocity structure for four areas, the differences between those averages, and selected 2D vertical profiles through the 3D model.

The first observation is variations in uppermost mantle velocities between the Archean and many of the younger terranes (Figures 3 and 4). From the Moho to about 100–150-km depth, shear-wave velocities in the lithospheric mantle beneath the Archean Kaapvaal and Zimbabwe cratons are $>2\%$ higher than beneath the Damara, Gariiep, Mozambique, Irumide, and Southern Irumide belts. Only part of the Namaqua-Natal Belt is imaged and therefore it is difficult to include this terrane in the comparison. Higher velocities in the uppermost mantle beneath Archean compared to younger terranes has been documented in other continents and attributed to the depletion of basaltic components (mainly Fe) (Fouch et al., 2004; Jordan, 1979; Schutt & Leshner, 2010), but comparable differences in uppermost mantle velocities have not been previously well imaged in southern Africa. In the continental-scale models of Emry et al. (2019) and Fishwick (2010), e.g., velocities at around 100-km depth beneath the Damara Belt are fairly similar to the velocities beneath the Kaapvaal and Zimbabwe cratons.

The next observation is about the thickness of cratonic lithosphere (Figures 3 and 4). There has been significant debate about the depth extent of the lithospheric mantle under the Kaapvaal and Zimbabwe cratons, with seismic-derived estimates ranging from ~ 150 to >300 km (e.g., Hansen et al., 2009; Kumar et al., 2007; Ravenna et al., 2018; Wang et al., 2008; Wittlinger & Farra, 2007). Our model shows that at depths of 250 km and greater there is less than a 1% difference in velocities between craton and off-craton areas (Figures 3 and 4), with shear-wave velocities everywhere between 4.7 and 4.8 km/s. This finding corroborates previous estimates of cratonic lithosphere thickness in the 200–250-km depth range for southern Africa (e.g., Adams & Nyblade, 2011; Fishwick, 2010; Priestley et al., 2008).

The third observation is variations in velocities that illuminate the edges of the Kalahari Craton lithosphere. Our model shows, to depths of about 200 km, higher velocities extending from the core of the cratonic nucleus (i.e., Kaapvaal and Zimbabwe cratons) to the west beneath the Kheis and Rehoboth terranes and to the north and northwest beneath the Okwa and Magondi terranes. At 200-km depth, there is a marked change in velocities along the southern boundary of the Damara Belt and western boundary of the Rehoboth Terrane, indicating that thick cratonic lithosphere is present to the south and east of those terrane boundaries, respectively. In other words, our models show that the northern boundary of the greater Kalahari Craton lies along the southern margin of the Damara Belt, and that the western boundary lies along the eastern margin of the Gariiep and Namaqua-Natal belts. This finding is consistent with body wave tomography models showing a similar transition in *P* wave and *S* wave velocity structure across these terrane boundaries (Ortiz et al., 2019; White-Gaynor et al., 2020), and also with MT studies (Miensopust et al., 2011; Muller et al., 2009).

The final observation concerns the presence of thermally perturbed upper mantle providing buoyant support for plateau uplift across southern Africa. As noted in Section 2, some authors argue for the presence of thermally perturbed upper mantle (i.e., Li & Burke, 2006), while others argue against any current thermal modification of the upper mantle (Adams & Nyblade, 2011). In comparing the velocity structure of the

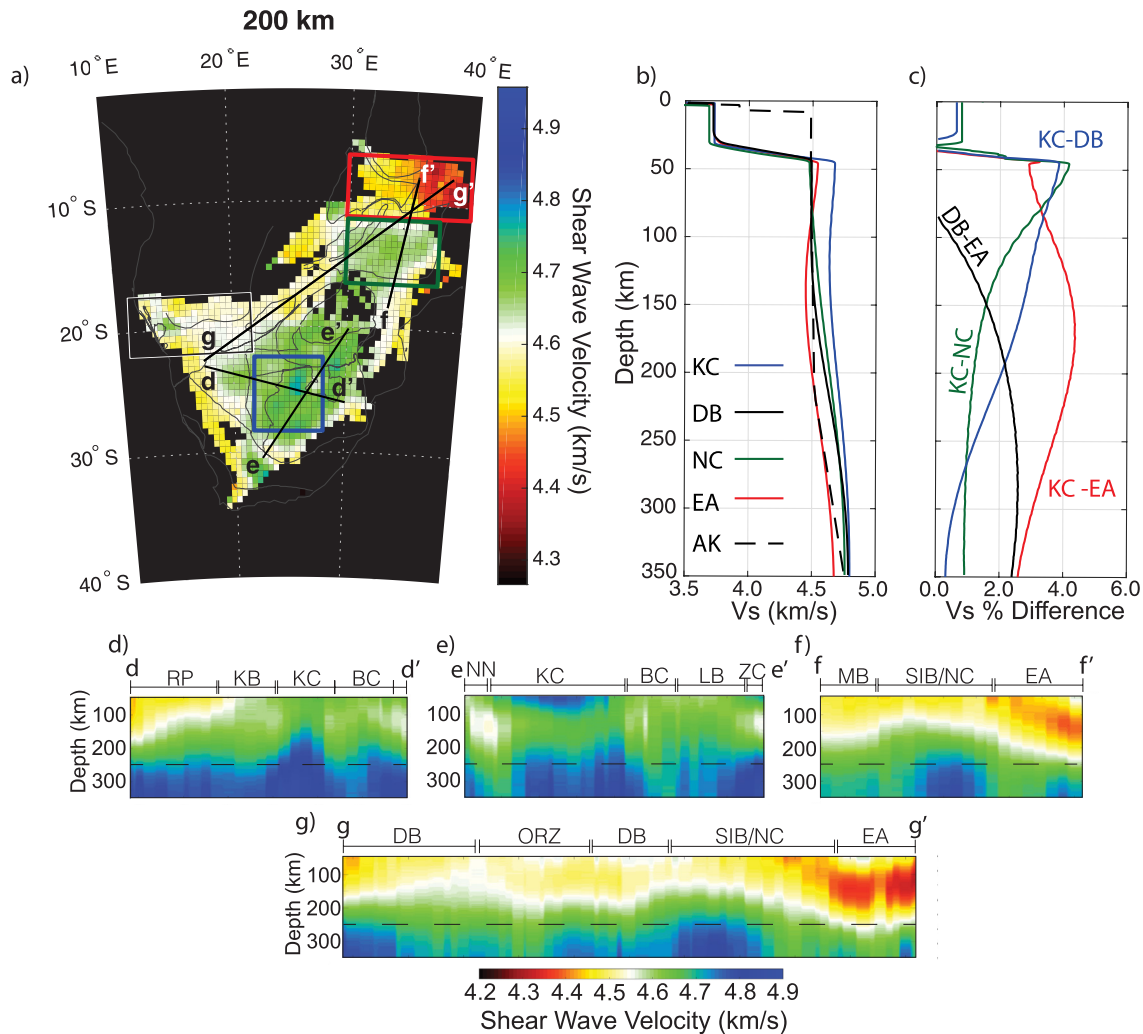


Figure 4. (a) 200-km depth cross-section through the 3D shear-wave velocity model. Areas used to calculate regional average 1D velocity models shown in colored rectangles. KC, Kalahari Craton (blue rectangle); DB, Damara Belt (black rectangle); EA, East Africa (red rectangle); NC, Niassa Craton (green rectangle). (b) Average 1D velocity profiles calculated for the regions boxed in (a). AK, AK135 (Kennett et al., 1995). (c) Percent shear-wave velocity difference between 1D velocity profiles in (b). (d)–(g) Vertical profiles through the shear-wave velocity model. Profile locations are shown in (a). The velocity scale for vertical profiles is shown below (g). Terrain boundaries are shown above the profiles. RP, Rehoboth Province; KB, Kheis Belt; KC, Kaapvaal Craton; BC, Bushveld Complex; NN, Namaqua-Natal Belt; LB, Limpopo Belt; MB, Mozambique Belt in Mozambique; SIB/NC, Southern Irumide Belt/Niassa Craton; EA, Mozambique Belt in East Africa; DB, Damara Belt; ORZ, Okavango Rift Zone. The black dashed reference line in each profile is at a depth of 250 km.

upper mantle beneath the Damara Belt and the Kalahari Craton to eastern Africa (Figures 3 and 4), there is little evidence for thermally perturbed (i.e., low shear-wave velocities) upper mantle beneath the uplifted parts of southern Africa, including the off-craton regions to the north and west of the greater Kalahari Craton. Shear-wave velocities are even notably higher than the global average (AK135) everywhere across southern Africa where elevations exceed about 1 km (Figure 1). The one area where our model does suggest the presence of thermally perturbed upper mantle is beneath the southern extension of the EARS in northern and central Mozambique. However, that part of southern Africa is not topographically elevated (Figure 1) and therefore not considered part of the Southern African Plateau. The lack of evidence for thermally perturbed upper mantle structure beneath the Southern African Plateau suggests that the present-day buoyant support for the plateau likely resides at midmantle or lower mantle depths.

As mentioned in Section 1, the uplift history of the Southern African Plateau and the origin of the uplift have received considerable attention (e.g., Bell et al., 2003; Griffin et al., 2014; Nyblade & Sleep, 2003). Nyblade and Sleep (2003) showed that thermal anomalies in the upper mantle from plume heads are not

likely to persist for 10s of millions of years, and therefore if plumes in the Cretaceous provided the source of buoyancy for the Cretaceous uplift, in addition to causing kimberlite eruptions and east-west tilting of the land surface, there would not likely remain any evidence of those plumes in the velocity structure of the upper mantle today. Therefore, the results of our study provide little insight into the origin of uplift of southern Africa during Mesozoic times, or even during mid-Cenozoic times.

With regard to the source of buoyancy for the Southern African Plateau today, and also possibly over the past few million years, we reiterate that our results show little evidence for thermal modification of the upper mantle. Thus, the source of buoyancy supporting the present-day plateau topography and any uplift that may have occurred over the past few million years likely resides at midmantle to lower mantle depths, a finding consistent with previous studies arguing that the buoyant support for the plateau, at least today, comes from the African Superplume structure within the midmantle to lower mantle.

7. Summary and Conclusions

We have developed the first 3D shear velocity model for southern Africa from Rayleigh wave tomography that utilizes regional network data spanning the entire subcontinent, from Namibia in the west to Mozambique in the east. Rayleigh waves from 499 teleseismic events have been used with the ASWMS workflow to obtain phase velocity maps from periods of 30–200 s. 1D shear-wave velocity models, obtained by inverting dispersion curves for $0.5^\circ \times 0.5^\circ$ cells extracted from the phase velocity maps, have been combined to create a 3D model.

The models show high velocities (~ 4.7 – 4.8 km/s) at depths of 50–250 km beneath the Archean terranes (Kaaopvaal, Zimbabwe, Limpopo) in southern Africa, as well as the Paleoproterozoic Kheis and Rehoboth terranes, and the Mesoproterozoic Okwa and Magondi terranes, indicating that the margin of the greater Kalahari Craton, as defined by the presence of high velocity upper mantle extending to depths of 150–200 km, lies along the southern boundary of the Damara Belt and the eastern boundaries of the Gariep and Namaqua-Natal belts. At depths ≥ 250 km, there is little difference in the shear-wave velocity structure beneath the craton and off-craton regions, suggesting that the cratonic lithosphere extends to depths of about 200–250 km. Upper mantle velocities beneath all of the uplifted areas of southern Africa are higher than the global average and significantly higher than beneath eastern Africa, implying that there is little, if any, thermal modification of the upper mantle beneath the Southern African Plateau today. Buoyant support for the plateau therefore likely resides in the midmantle to lower mantle.

Data Availability Statement

Data from seismic stations used in this study come from the following open networks at the IRIS data management center (<http://ds.iris.edu/ds/>), the 2015–2018 AfricaArray Namibia network (https://doi.org/10.7914/SN/8A_2015), the 2010–2012 Walpass network (<https://doi.org/10.14470/1N134371>), the permanent GEOFON station at Windhoek (<https://doi.org/10.14470/TR560404>), the SAFARI network (https://doi.org/10.7914/SN/XK_2012), the Botswana Network of Autonomously Recording Seismographs (<https://doi.org/10.7914/SN/NR>), the AfricaArray Uganda/Tanzania/Zambia network (https://doi.org/10.7914/SN/ZP_2007), The Study of Extension and Magmatism in Malawi and Tanzania (SEGMeNT) project (https://doi.org/10.7914/SN/YQ_2013), the Global Seismic Network (<https://doi.org/10.7914/SN/II>, <https://doi.org/10.7914/SN/IU>, <https://doi.org/10.7914/SN/GT>, <https://doi.org/10.7914/SN/ID>); the Mozambique Rift Tomography (MOZART) project; the SASE network (https://doi.org/10.7914/SN/XA_1997).

References

- Accardo, N., Gaherty, J., Shillington, D., Ebinger, C., Nyblade, A., Mbogoni, G., et al. (2017). Surface-wave imaging of the weakly-extended Malawi Rift from ambient-noise and teleseismic Rayleigh waves from onshore and lake-bottom seismometers. *Geophysical Journal International*, 209, 1892–1905. <https://doi.org/10.1093/gji/ggx133>
- Accardo, N. J., Gaherty, J. B., Shillington, D. J., Hopper, E., Nyblade, A. A., Ebinger, C. J., et al. (2020). Thermochemical modification of the upper mantle beneath the Northern Malawi Rift constrained from shear velocity imaging. *Geochemistry, Geophysics, Geosystems*, 21, e2019GC008843. <https://doi.org/10.1029/2019GC008843>
- Adams, A., & Nyblade, A. (2011). Shear wave velocity structure of the southern African upper mantle with implications for the uplift of southern Africa. *Geophysical Journal International*, 186(2), 808–824. <https://doi.org/10.1111/j.1365-246X.2011.05072.x>

Acknowledgments

This work was supported by grant ALW-GO-AO/11-30 provided by Nederlandse Organisatie voor Wetenschappelijk Onderzoek (NWO) and National Science Foundation grants 0440032, 0530062, 0824781, 1128936, and 1634108. We acknowledge the efforts of staff at the Botswana Geological Survey and Namibia Geological Survey for installing and maintaining seismic stations, and we would like to thank Joao Fonseca and an anonymous reviewer for constructive and helpful comments.

- Baby, G., Guillocheau, F., Braun, J., Robin, C., & Dall'Asta, M. (2020). Solid sedimentation rates history of the Southern African continental margins: Implications for the uplift history of the South African Plateau. *Terra Nova*, 32(1), 53–65. <https://doi.org/10.1111/ter.12435>
- Begg, G. C., Griffin, W. L., Natapov, L. M., O'Reilly, S. Y., Grand, S. P., O'Neill, C. J., et al. (2009). The lithospheric architecture of Africa: Seismic tomography, mantle petrology, and tectonic evolution. *Geosphere*, 5(1), 23–50. <https://doi.org/10.1130/GES00179.1>
- Bell, D. R., Schmitz, M. D., & Janney, P. E. (2003). Mesozoic thermal evolution of the southern African mantle lithosphere. *Lithos*, 71(2–4), 273–287. [https://doi.org/10.1016/S0024-4937\(03\)00117-8](https://doi.org/10.1016/S0024-4937(03)00117-8)
- Braun, J., Guillocheau, F., Robin, C., Baby, G., & Jelsma, H. (2014). Rapid erosion of the Southern African Plateau as it climbs over a mantle superswell. *Journal of Geophysical Research: Solid Earth*, 119, 6093–6112. <https://doi.org/10.1002/2014JB010998>
- Chevrot, S., & Zhao, L. (2007). Multiscale finite-frequency Rayleigh wave tomography of the Kaapvaal craton. *Geophysical Journal International*, 169(1), 201–215. <https://doi.org/10.1111/j.1365-246X.2006.03289.x>
- De Wit, M. J., de Ronde, C. E., Tredoux, M., Roering, C., Hart, R. J., Armstrong, R. A., et al. (1992). Formation of an Archaean continent. *Nature*, 357, 553–562.
- Domingues, A., Silveira, G., Ferreira, A. M., Chang, S. J., Custódio, S., & Fonseca, J. F. (2016). Ambient noise tomography of the East African Rift in Mozambique. *Geophysical Journal International*, 204(3), 1565–1578. <https://doi.org/10.1093/gji/ggv538>
- Emry, E. L., Shen, Y., Nyblade, A. A., Flinders, A., & Bao, X. (2019). Upper mantle Earth structure in Africa from full-wave ambient noise tomography. *Geochemistry, Geophysics, Geosystems*, 20, 120–147. <https://doi.org/10.1029/2018GC007804>
- Fadel, I., Paulssen, H., van der Meijde, M., Kwadiba, M., Ntibinyane, O., Nyblade, A., & Durrheim, R. (2020). Crustal and upper mantle shear wave velocity structure of Botswana: The 3 April 2017 central Botswana earthquake linked to the East African Rift System. *Geophysical Research Letters*, 47, e2019GL085598. <https://doi.org/10.1029/2019GL085598>
- Fishwick, S. (2010). Surface wave tomography: Imaging of the lithosphere–asthenosphere boundary beneath central and southern Africa? *Lithos*, 120(1–2), 63–73. <https://doi.org/10.1016/j.lithos.2010.05.011>
- Fouch, M. J., James, D. E., VanDecar, J. C., & Van der Lee, S., & Kaapvaal Seismic Group. (2004). Mantle seismic structure beneath the Kaapvaal and Zimbabwe Cratons. *South African Journal of Geology*, 107(1–2), 33–44. <https://doi.org/10.2113/107.1-2.33>
- Frimmel, H. E., & Frank, W. (1998). Neoproterozoic tectono-thermal evolution of the Gariep Belt and its basement, Namibia and South Africa. *Precambrian Research*, 90(1–2), 1–28. [https://doi.org/10.1016/S0301-9268\(98\)00029-1](https://doi.org/10.1016/S0301-9268(98)00029-1)
- Gee, L. S., & Jordan, T. H. (1992). Generalized seismological data functionals. *Geophysical Journal International*, 111(2), 363–390. <https://doi.org/10.1111/j.1365-246X.1992.tb00584.x>
- Griffin, W. L., Batumike, J. M., Greau, Y., Pearson, N. J., Shee, S. R., & O'Reilly, S. Y. (2014). Emplacement ages and sources of kimberlites and related rocks in southern Africa: U–Pb ages and Sr–Nd isotopes of groundmass perovskite. *Contributions to Mineralogy and Petrology*, 168(1), 1032. <https://doi.org/10.1007/s00410-014-1032-4>
- Gurnis, M., Mitrovica, J. X., Ritsema, J., & van Heijst, H. J. (2000). Constraining mantle density structure using geological evidence of surface uplift rates: The case of the African superplume. *Geochemistry, Geophysics, Geosystems*, 1(7), 1020. <https://doi.org/10.1029/1999GC000035>
- Hansen, S., Nyblade, A., Julia, J., Dirks, P., & Durrheim, R. (2009). Upper-mantle low-velocity zone structure beneath the Kaapvaal craton from S-wave receiver functions. *Geophysical Journal International*, 178, 1021–1027. <https://doi.org/10.1111/j.1365-246X.2009.04178.x>
- Hanson, R. E. (2003). Proterozoic geochronology and tectonic evolution of southern Africa. *Geological Society, London, Special Publications*, 206(1), 427–463. <https://doi.org/10.1144/GSL.SP.2003.206.01.20>
- Herrmann, R. B. (2013). Computer programs in seismology: An evolving tool for instruction and research. *Seismological Research Letters*, 84(6), 1081–1088.
- James, D. E., Fouch, M. J., VanDecar, J. C., & Van Der Lee, S., & Kaapvaal Seismic Group. (2001). Tectospheric structure beneath southern Africa. *Geophysical Research Letters*, 28(13), 2485–2488. <https://doi.org/10.1029/2000GL012578>
- Jelsma, H. A., & Dirks, P. H. (2002). Neoarchaean tectonic evolution of the Zimbabwe Craton. *Geological Society, London, Special Publications*, 199(1), 183–211. <https://doi.org/10.1144/GSL.SP.2002.199.01.10>
- Jin, G., & Gaherty, J. B. (2015). Surface wave phase-velocity tomography based on multichannel cross-correlation. *Geophysical Journal International*, 201(3), 1383–1398. <https://doi.org/10.1093/gji/ggv079>
- Jin, G., Gaherty, J. B., Abers, G. A., Kim, Y., Eilon, Z., & Buck, W. R. (2015). Crust and upper mantle structure associated with extension in the Woodlark Rift, Papua New Guinea from Rayleigh-wave tomography. *Geochemistry, Geophysics, Geosystems*, 16, 3808–3824. <https://doi.org/10.1002/2015GC005840>
- Jordan, T. H. (1979). Mineralogies, densities and seismic velocities of garnet lherzolites and their geophysical implications. In F. Boyd, & H. O. Meyer (Eds.), *The mantle sample: Inclusion in kimberlites and other volcanics* (Vol. 16, pp. 1–14). American Geophysical Union. <https://doi.org/10.1029/SP016p0001>
- Kachingwe, M., Nyblade, A., & Julia, J. (2015). Crustal structure of Precambrian terranes in the southern African subcontinent with implications for secular variation in crustal genesis. *Geophysical Journal International*, 202(1), 533–547. <https://doi.org/10.1093/gji/ggv136>
- Kennett, B. L., Engdahl, E. R., & Buland, R. (1995). Constraints on seismic velocities in the Earth from traveltimes. *Geophysical Journal International*, 122(1), 108–124. <https://doi.org/10.1111/j.1365-246X.1995.tb03540.x>
- Kumar, P., Yuan, X., Ravi Kumar, M., Kind, R., Li, X., & Chadha, R. (2007). The rapid drift of the Indian tectonic plate. *Nature*, 449, 894–897. <https://doi.org/10.1038/nature06214>
- Li, A. (2011). Shear wave model of southern Africa from regional Rayleigh wave tomography with 2-D sensitivity kernels. *Geophysical Journal International*, 185, 832–844. <https://doi.org/10.1111/j.1365-246X.2011.04971.x>
- Li, A., & Burke, K. (2006). Upper mantle structure of southern Africa from Rayleigh wave tomography. *Journal of Geophysical Research*, 111, B10303. <https://doi.org/10.1029/2006JB004321>
- Lin, F.-C., & Ritzwoller, M. H. (2011). Helmholtz surface wave tomography for isotropic and azimuthally anisotropic structure. *Geophysical Journal International*, 186(3), 1104–1120. <https://doi.org/10.1111/j.1365-246X.2011.05070.x>
- Miensopust, M. P., Jones, A. G., Muller, M. R., Garcia, X., & Evans, R. L. (2011). Lithospheric structures and Precambrian terrane boundaries in northeastern Botswana revealed through magnetotelluric profiling as part of the Southern African Magnetotelluric Experiment. *Journal of Geophysical Research*, 116, B02401. <https://doi.org/10.1029/2010JB007740>
- Muller, M. R., Jones, A. G., Evans, R. L., Grütter, H. S., Hatton, C., Garcia, X., et al. (2009). Lithospheric structure, evolution and diamond prospectivity of the Rehoboth Terrane and western Kaapvaal Craton, southern Africa: Constraints from broadband magnetotellurics. *Lithos*, 112, 93–105. <https://doi.org/10.1016/j.lithos.2009.06.023>
- Nyblade, A. A., & Robinson, S. W. (1994). The African superswell. *Geophysical Research Letters*, 21(9), 765–768. <https://doi.org/10.1029/94GL00631>

- Nyblade, A. A., & Sleep, N. H. (2003). Long lasting epeirogenic uplift from mantle plumes and the origin of the Southern African Plateau. *Geochemistry, Geophysics, Geosystems*, 4(12), 1105. <https://doi.org/10.1029/2003GC000573>
- Ortiz, K., Nyblade, A., van der Meijde, M., Paulssen, H., Kwadiba, M., Ntubinyane, O., et al. (2019). Upper mantle P-and S-wave velocity structure of the Kalahari Craton and surrounding Proterozoic terranes, southern Africa. *Geophysical Research Letters*, 46, 9509–9518. <https://doi.org/10.1029/2019GL084053>
- Priestley, K., McKenzie, D., Debayle, E., & Pilidou, S. (2008). The African upper mantle and its relationship to tectonics and surface geology. *Geophysical Journal International*, 175(3), 1108–1126. <https://doi.org/10.1111/j.1365-246X.2008.03951.x>
- Ravenna, M., Lebedev, S., Fulla, J., & Adam, J. M. C. (2018). Shear-wave velocity structure of Southern Africa's lithosphere: Variations in the thickness and composition of cratons and their effect on topography. *Geochemistry, Geophysics, Geosystems*, 19, 1499–1518. <https://doi.org/10.1029/2017GC007399>
- Schutt, D. L., & Leshner, C. E. (2010). Compositional trends among Kaapvaal Craton garnet peridotite xenoliths and their effects on seismic velocity and density. *Earth and Planetary Science Letters*, 300(3–4), 367–373. <https://doi.org/10.1016/j.epsl.2010.10.018>
- Sebai, A., Stutzmann, E., Montagner, J. P., Sicilia, D., & Beucler, E. (2006). Anisotropic structure of the African upper mantle from Rayleigh and Love wave tomography. *Physics of the Earth and Planetary Interiors*, 155(1–2), 48–62. <https://doi.org/10.1016/j.pepi.2005.09.009>
- Stanley, J. R., Braun, J., Baby, G., Guillocheau, F., Robin, C., Flowers, R., et al. (2020). Constraining plateau uplift in southern Africa by combining thermochronology, sediment flux, topography, and landscape evolution modeling. *Earth and Space Science Open Archive*, 67. <https://doi.org/10.1002/essoar.10504712.1>
- Stanley, J. R., Flowers, R. M., & Bell, D. R. (2013). Kimberlite (U-Th)/He dating links surface erosion with lithospheric heating, thinning, and metasomatism in the southern African Plateau. *Geology*, 41(12), 1243–1246. <https://doi.org/10.1130/G34797.1>
- Stanley, J. R., Flowers, R. M., & Bell, D. R. (2015). Erosion patterns and mantle sources of topographic change across the southern African Plateau derived from shallow and deep records of kimberlites. *Geochemistry, Geophysics, Geosystems*, 16(9), 3235–3256. <https://doi.org/10.1002/2015GC005969>
- Tugume, F., Nyblade, A., Julià, J., & van der Meijde, M. (2013). Precambrian crustal structure in Africa and Arabia: Evidence lacking for secular variation. *Tectonophysics*, 609, 250–266. <https://doi.org/10.1016/j.tecto.2013.04.027>
- Wang, Y., Wen, L., & Weidner, D. (2008). Upper mantle SH- and P-velocity structures and compositional models beneath southern Africa. *Earth and Planetary Science Letters*, 267, 596–608. <https://doi.org/10.1016/j.epsl.2007.12.010>
- Weatherall, P., Marks, K. M., Jakobsson, M., Schmitt, T., Tani, S., Arndt, J. E., et al. (2015). A new digital bathymetric model of the world's oceans. *Earth and Space Science*, 2, 331–345. <https://doi.org/10.1002/2015EA000107>
- White-Gaynor, A., Nyblade, A., Durrheim, R., Raveloson, R., van der Meijde, M., Fadel, I., et al. (2020). Lithospheric boundaries and upper mantle structure beneath southern Africa imaged by P- and S-wave velocity models. *Geochemistry, Geophysics, Geosystems*, 21, e2020GC008925. <https://doi.org/10.1029/2020GC008925>
- Wittlinger, G., & Farra, V. (2007). Converted waves reveal a thick and layered tectosphere beneath the Kalahari super-craton. *Earth and Planetary Science Letters*, 254, 404–415. <https://doi.org/10.1016/j.epsl.2006.11.048>
- Youssof, M., Thybo, H., Artemieva, I. M., & Levander, A. (2015). Upper mantle structure beneath southern African cratons from seismic finite-frequency P-and S-body wave tomography. *Earth and Planetary Science Letters*, 420, 174–186. <https://doi.org/10.1016/j.epsl.2015.01.034>